Journal of King Saud University - Science 36 (2024) 103524

HOSTED BY

Contents lists available at ScienceDirect

Journal of King Saud University - Science

journal homepage: www.sciencedirect.com

Full Length Article

Geochemical study of Ambaji – Sendra granitoids and mafic dykes from the South Delhi fold belt, NW Indian shield: Implications for magma generation, emplacement and geodynamic evolution

Saima Rahman [a,*], M. Shamim Khan [a], Mohammed S. Fnais [b], Tavheed Khan [c]

[a] Department of Geology, Aligarh Muslim University, Aligarh 202002, India
[b] Department of Geology and Geophysics, College of Science, King Saud University, Riyadh 11451, Saudi Arabia
[c] CSIR-National Geophysical Research Institute, Hyderabad, India

ARTICLE INFO

Keywords:
South Delhi Fold belt
Aravalli craton
NW Indian shield
Rodinia connection

ABSTRACT

This study presents a comprehensive account of geochemical data on the granitoids of Ambaji-Sendra Terrain and associated mafic dykes. These granitoids, interpreted as S–type, I-type and A-type, lack a consensual interpretation probably due to the study of only those rocks which are exposed in Sendra region. We identified that these granitoids are A-type (A2- subtype) granites. There are two petrogenetic groups of the granitoids having exclusive crustal and crust-mantle interactive origins which are supported by their mineralogy and structure. The associated dykes also display two distinct geochemical groups one with within-plate character and other with typical arc signatures. Whole body of evidence suggests that magma for the granitoids and dykes was generated during the closure of Delhi Ocean. The simultaneous emplacement of granitoids started during subduction process and culminated after the collision or/ accretion of Delhi arc with eastern crustal block, consequent to the Rodinian assembly mechanism.

1. Introduction

Granitoids record formation and evolution of the continental crust (Kemp et al., 2007). The composition and structure of lithosphere is effected by the process of generation and emplacement of granitoids. The NW Indian shield inhabited in Aravalli craton experienced Aravalli and Delhi orogenies. During Delhi orogeny, ophiolite was formed (Khan et al., 2005) with simultaneous emplacement of numerous voluminous granitoids (Pandit et al., 2003). These granitoids are exposed in a linear belt called Ambaji – Sendra belt/terrain. These Neoproterozoic (990–970 Ma) granitoids considered to have formed/emplaced during Rodinian assembly, are variably interpreted as S – type (Bhattacharjee et al., 1988), I-type (Pandit et al., 2003) and A-type (Tiwana et al., 2022). Thus a proper knowledge of tectonics and petrogenesis of these granitoids will improve our understanding about the evolution of the continental lithosphere in this part of Indian shield. Present study is an attempt for this aspect wherein new geochemical data on the granitoids in conjunction with their mafic dykes have been interpreted (see Table 1A).

2. Geological setup

The ENE–WSW- trending Central Indian Tectonic zone, a Proterozoic suture, divides the Indian Shield into north and south cratonic blocks (Fig. 1a). The Aravalli Mountain Range (AMR), located in the northern block, is one of the oldest mountain ranges of the world. It extends from Delhi in the north to Gujarat in the south (>700 km length and 20–200 km width) with general NE-SW trend (Heron, 1953). It is terminated by Great Boundary Fault in the east and Western Marginal Fault in the west (Fig. 1b). AMR preserves complete Precambrian rock record with excellent exposures. Archean basement and two main unconformity-bound Proterozoic Aravalli and Delhi supracrustal sequences are three major stratigraphic units of AMR.

Archean basement is designated as Banded Gneiss Complex (BGC) due to its excellently preserved lithocomponents in banded form (Heron, 1953). BGC, a 3.3 Ga old terrain (Gopalan et al. 1990) consists of amphibolite to granulite grade, tonalitic to granodioritic gneisses, with associated lenticular masses of amphibolites (Heron, 1953). BGC is unconformably overlain by Paleo to Mesoproterozoic Aravalli Supergroup and Meso to Neoproterozoic Delhi Supergroup which constitute Aravalli

* Corresponding author.
E-mail address: saimarahman19594@gmail.com (S. Rahman).

https://doi.org/10.1016/j.jksus.2024.103524
Received 27 August 2024; Received in revised form 3 November 2024; Accepted 4 November 2024
Available online 5 November 2024

Table 1A
Geographical locations of geochemically analyzed samples.

A	Sample Field Code	Latitude	Longitude
Tarpal	Sample 15(a)	24^0 49 17.126N	73^0 25 53.941E
	Sample 15(b)	24^0 49 17.126N	73^0 25 53.941E
	Sample 15(c)	24^0 49 17.126N	73^0 25 53.941E
Ranakpur	Sample 16	25^0 06 48.190N	73^0 28 15.280E
	Sample 16(b)	25^0 06 48.190N	73^0 28 15.280E
	Sample 16(c)	25^0 06 48.190N	73^0 28 15.280E
Jaitpura	Sample 18	26^0 04 32.419N	74^0 08 48.966E
	Sample 18(b)	26^0 04 36.186N	74^0 08 48.903E
Borwar	Sample 19(a)	26^0 04 21.631N	74^0 14 48.519E
	Sample 19(b)	26^0 04 21.176N	74^0 11 46.472E
	Sample 19(c)	26^0 04 21.176N	74^0 11 46.472E
	Sample 19(d)	26^0 04 15.751N	74^0 11 39.572E
	Sample 19(e)	26^0 04 13.687N	74^0 11 38.645E
	Sample 19(d')	26^0 04 15.751N	74^0 11 39.572E
Seliberi	Sample 20(c)	26^0 02 53.145N	74^0 09 43.377E
	Sample 20(d)	26^0 02 53.145N	74^0 09 43.377E
	Sample 20(e)	26^0 02 53.145N	74^0 09 43.377E
	Sample 20(f)	26^0 02 58.551N	$74^0$1154.427E
Vagdadi	Sample 25(a)	$24^0$1619.226N	$72^0$3443.920E
	Sample 25(c)	$24^0$1620.897N	$72^0$3444.835E
	Sample 25(e)	$24^0$1620.897N	$72^0$3444.835E
Chitar	Sample 21(a)	26^0 05 21.250N	74^0 11 52.932E
	Sample 21(b)	26^0 05 21.059N	74^0 11 49.625E
	Sample 21(c)	26^0 05 21.059N	74^0 11 49.625E
Chang	Sample 22(a)	26^0 04 40.840N	74^0 12 20.216E
	Sample 22(b)	26^0 04 40.840N	74^0 12 20.216E
	Sample 22(c)	26^0 04 40.840N	74^0 12 20.216E
	Sample 22(d)	26^0 04 40.840N	74^0 12 20.216E
Balaram	Sample 23(a)	24^0 15 27.884N	72^0 31 40.978E
	Sample 23(b)	24^0 15 27.884N	72^0 31 40.978E
	Sample 23(c)	24^0 15 27.884N	72^0 31 40.978E
Chiknawas	Sample 26(b)	24^0 17 23.217N	72^0 44 42.073E
	Sample 26(c)	24^0 17 23.217N	72^0 44 42.073E
	Sample 26(d)	24^0 17 23.217N	72^0 44 42.073E
	Sample 26(e)	24^0 17 23.217N	72^0 44 42.073E
	Sample 26(f)	24^0 17 23.217N	72^0 44 42.073E

and Delhi fold belts respectively (Gupta et al. 1997). Aravalli Supergroup is hosted in two linear belts named Udaipur (shallow water facies) and Jharol (deep water facies) belts. Eastern side of AMR is occupied by a Mesoproterozoic Vindhyan basin and western margin is surrounded by Trans Aravalli Region (TAR), a foreland basin (Heron, 1953) followed by Malani Igneous Province and Phanerozoic sediments.TAR is mainly comprised of post Delhi granites (Erinpura Granite Suite) and three linear isolated sedimentary basins namely Sirohi, Sindreth and Punagarh.

NE–SW, Meso- Neproterozoic Delhi fold belt is the main edifice of AMR with a cauliflower-like head and long linear tail. There is dichotomy in terms of sedimentation and tectonic evolution of Delhi fold belt (Sinha-Roy, 1988). Its northern cauliflower like segment (North Delhi fold belt –NDFB), outcropped between Delhi and Ajmer, and southern tail (South Delhi fold belt – SDFB) extending from Ajmer to Ahmedabad and overlying unconformably Aravalli fold belt, are considered to have deposited ~ 1.7 Ga and 1.2–1.0 Ga (U-Pb & Pb isotopic data) respectively, validated also by intrusive granitic plutons into sedimentary rocks i.e. 1.5–1.7 and 0.8 to 1.0 Ga respectively (Sm-Nd ages, Volpe and Macdougall, 1990).The SDFB has most complex geological setting in AMR due to multiple deformations (Roy and Jakhar, 2002) and hence lacks in a definite stratigraphic framework.

In SDFB, rocks of Delhi Supergroup are divided into two groups i.e. lower Gogunda Group (predominantly arenaceous) and upper Kumbhalgarh (calcareous cum argillaceous). SDFB rocks have suffered regional metamorphism, ranging from greenschist to granulite facies. SDFB have been divided into five longitudinal tectonic zones from west to east (Sen, 1980). Sinha-Roy (1988) established that SDFB is a subduction complex and its zones 1 and 2 constitute the youngest part, to which he named as Ambaji-Sendra terrain (AST) (Fig. 1c). Significant rock types of AST are mafic volcanics with adequate proportion of felsics along with metasediments. In AST, Kumbalgarh Group is represented by calc-gneiss, marble, calc-biotite schist, amphibolites and quartzite. Several granitoid plutons including Tarpal, Ranakpur, Chitar, Chang, Seliberi, Borwar, Jaitpura, Balaram and Chiknawas intrude the Kumbalgarh rocks of AST. Mineralogically, granitoids are divided into two groups, coarse to very coarse grained porphyritic and foliated with elongated phenocrysts of relatively smaller size. These granitoids have been intruded by mafic dykes. These dykes are few centimeter to several meters thick and are gabbroic, doleritic as well as volcanic often possessing amygdaloidal structure consisting of phenocryst (40 %) and matrix (60 %).

3. Sampling and analytical techniques

Thirty-Five fresh and unweathered samples of granites and dykes were screened for geochemical analysis. Major and trace elements have been analyzed at the CSIR-NGRI, Hyderabad by XRF Spectrometer and ICP-MS respectively. Established geochemical analyses protocol given in Balaram (2018) was followed. Accuracy and precision values were calculated using known and analyzed values of standard reference materials, G-2 (felsic rocks – major and trace elements), BHVO-1 (mafic rocks- major elements) and BHVO −2 (mafic rocks- trace elements). Average accuracy reported in RSD (Relative Standard Deviation) is better than 5 % for major elements and 3 % for trace elements and average precision for both major and trace elements generally varies between 0.03 % to 3.73 % RSD.

4. Ambaji Sendra Terrain granitoids

Primary frame work modes of granitoids are quartz, plagioclase and K–feldspars. Biotite and hornblende are other significant modes with variable proportions (Table 2). Sericite and epidote appear to be alteration product of biotite and feldspars. Main accessory minerals are muscovite, zircon, allanite, magnetite ± ilmenite, and apatite. Synthesis of the framework data reveals that although there is not much difference in modal mineralogy, the granitoids exposed at Chitar, Chang, Tarpal, Balaram and Chiknawas, in general, are relatively plagioclase rich and biotite and hornblende deficient. The highest plagioclase content in Ranakpur, absence of hornblende in Seliberi and Jaitpura but its presence in one sample of Tarpal granitoids are exceptions.

4.1. Element mobility assessment

The primary idea about the mobilization of various elements is adduced from LOI (loss on ignition values). Secondary minerals like epidote, zoisite, chlorite etc contain significant H_2O or carbonate minerals like calcite, dolomite etc release CO_2, both enhance LOI values. Rocks considered as being 'weathered' or 'metamorphosed' possess signatures such as abnormally high water contents or high LOI values (Hastie et al., 2007). The LOI values of all the granitoids range between 1.13 and 1.39 wt% except one sample each of Jaitpura (1.66 wt%) and Balaram (1.43 wt%) granitoids (Table 1B), which are consistent to their primary mineralogy (amphiboles and micas.).

Values of correlation coefficients of major oxides with SiO_2 are

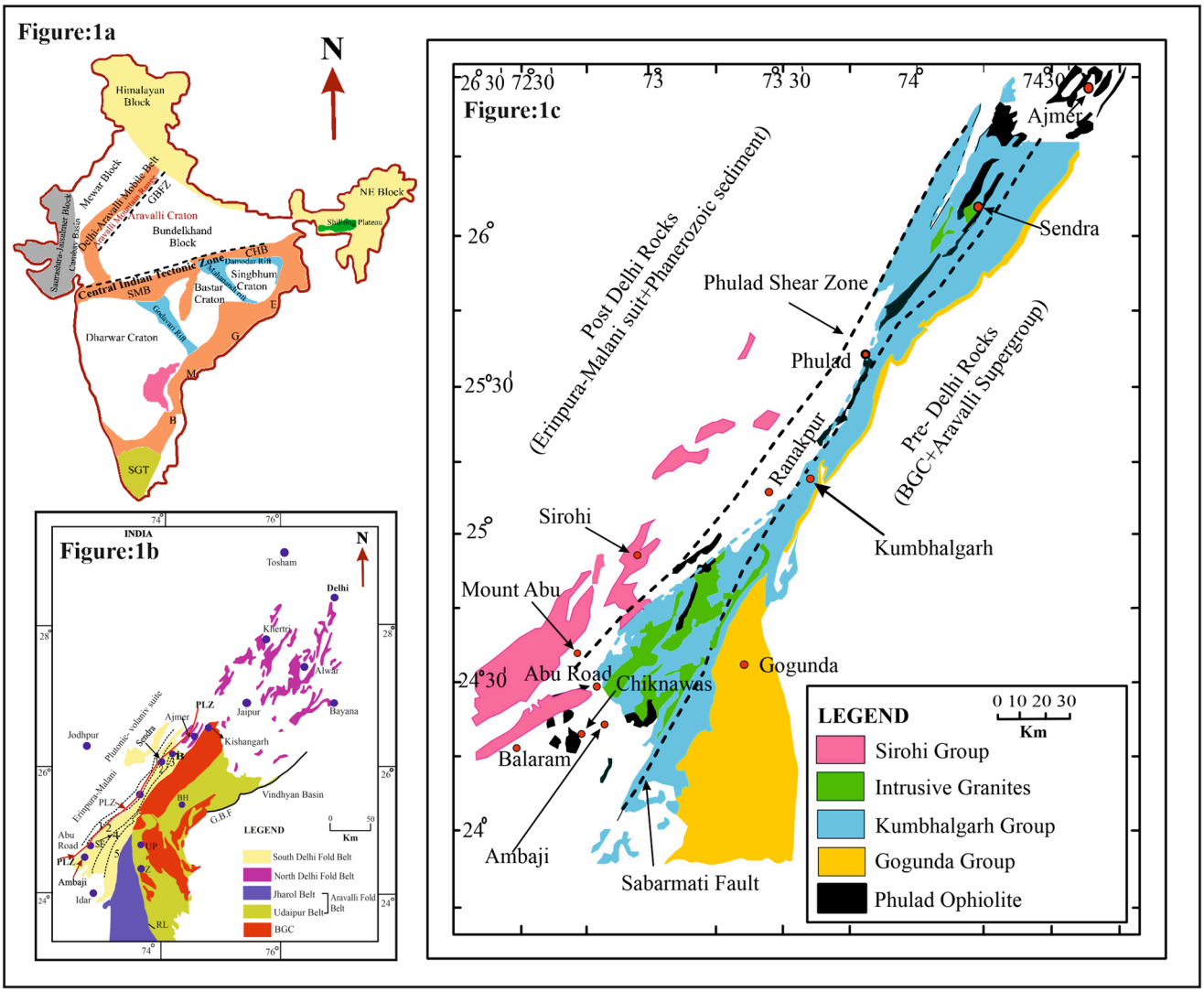

Fig. 1. (a) Map showing tectonic architecture of the Indian shield. SMB = Satpura Mobile Belt, EGMB = Eastern Ghat Mobile Belt, SGT = Southern Granulite Terrain, CHB = Chhotanagpur Belt and GBFZ = Great Boundary Fault Zone (Radhakrishna, 1989). (b)Simplified geological map of Aravalli-Delhi orogenic belt, (after Heron 1953; Gupta et al.1997). 1–5 longitudinal tectonic zones of Sen (1980). Index: B- Beawar, BH- Bhilwara; UP- Udaipur, Z – Zawar. GBF, Great Boundary Fault; SF, Sabarmati Fault; RL – Rakhabdev Lineament, PLZ – Phulad Lineament Zone. (c) Simplified geological map of Ambaji-Sendra terrain.

highly consistent in individual granitoids i.e. either positive or negative. For example, r coefficient of Al_2O_3 with SiO_2 is +0.99 in Tarpal, Jaitpura, Chitar, Chang and −0.89 to −0.99 (other granitoids). Na_2O and K_2O follow similar trend ruling out their any significant mobility. LILEs are also suspected for their mobility. When correlated with immobile element Zr, these elements also show their positive or negative variation within permissible limits −0.99 to +0.47 in consonances to their major oxides. Another noteworthy correlation is between Zr – Sc. Except Chitar granitoids all other granitoids have highly positive values (0.86 to 0.99). These correlations suggest that they are the source characteristics (Supplementary Table 1). Presence of allanite and zircon may increase concentration of REE and U, Th and Hf. Zr shows positive covariation with Hf, U, Th and Yb and Y with Ce in Borwar, Chitar and Chang granitoids. Despite such variations Th, U, HREE or Ce concentrations in these granitoids are not proportionally (anomalously) high with compatible concentrations of Zr or Y contents. It suggests that primary concentrations of REEs, U or Th have not been appreciably enhanced.

4.2. Geochemistry of AST granitoids

Tarpal, Balaram and Chiknawas granitoids show slightly wide range of all major oxides e.g. 61.80–70.92 wt%$_{SiO2}$,11.13–15.96 wt %$_{Al2O3}$(Tarpal),70.76–74.65 wt%$_{SiO2}$,11.28–14.63 wt%$_{Al2O3}$ (Balaram) and 70.28–76.54 wt% $_{SiO2}$,12.89–16.58 wt%$_{Al2O3}$(Chiknawas) whereas Jaitpura, Borwar, Seliberi, Chitar and Chang granitoids have very narrow range of major oxide contents, in particular SiO_2:73.66–77.34 wt% and Al_2O_3:11.82–13.89 wt%. Tarpal, Rankapur and Jaitpura granitoids are characterized by low Ga/Al ratio (1.61–2.81) coupled with small concentration of HFSE (Nb + Y:14.31–6.68) except Jaitpura possessing high (Nb + Y) content (113.4–158.2). Ga/Al ratio and (Nb + Y) content of Borwar, Seliberi, Chang, Chitar and Chicknawas granitoids are relatively high (3.11–3.91) and (129.61–242.35) respectively except Chiknawas which has intermediate (Nb + Y) content (43.97–65.52).

4.3. Classification of AST granitoids

The TAS and IUGS-based QAP classification schemes classify all AST granitoids as granites except Ranakpur and one sample of Tarpal as diorite and granodiorite respectively.

In regards to Fe number {FeO^T/ (FeO^T + MgO), Tarpal granites are magnesian (0.42–0.65), Ranakpur, Jaitpura, Seliberi, Chang and Balaram granitoids are ferroan (>0.8) and Borwar, Chitar and

Table 1B&C

Selected elemental ratios of Ambaji-Sendra Terrain granitoids(B) and Dykes(C). Eu/Eu* = $\{Eu_N/(Sm_N \times Gd_N)^{1/2}\}$. Normalizing values after Sun and McDonough (1989).

B	Tarpal			Ranakpur	Jaitpura		Borwar		
Field Code	15 (a)	15 (b)	15 (c)	16	18	18(b)	19(a)	19(c)	19(d)
Processing Code	TA 1	TA 2	TA 3	RA 1	JA 1	JA 2	BO 1	BO 2	BO 3
LOI	1.32	1.37	1.36	1.25	1.66	1.32	1.21	1.32	1.24
Th/U	7.27	12.56	12.02	1.91	7.65	6.58	8.64	7.07	4.03
Rb/Sr	1.43	0.37	0.30	0.06	3.02	3.56	0.77	0.74	1.70
Th/Sc	1.24	15.95	9.65	0.02	2.39	2.62	4.39	5.21	5.13
La/Sc	2.88	16.40	21.06	0.17	5.32	4.26	10.69	6.84	15.53
ΣREE	167.36	168.45	167.55	43.93	178.83	177.75	432.77	296.04	328.78
$(La/Yb)_N$	7.18	15.00	31.55	0.91	1.56	1.12	3.83	1.98	1.18
$(La/Sm)_N$	3.59	5.60	3.70	1.07	1.79	1.46	2.70	2.26	1.31
$(Gd/Yb)_N$	1.34	1.57	4.55	0.83	0.81	0.81	1.08	0.75	0.81
Eu/Eu*	0.63	0.70	1.21	0.89	0.24	0.24	0.40	0.41	0.44
Y/Nb	2.38	1.88	4.08	6.41	9.06	14.40	4.26	3.72	7.78
ASI	0.55	1.21	1.26	0.81	1.20	1.10	1.03	1.05	1.07
Ga/Al	2.40	2.29	1.61	2.26	2.81	2.74	3.11	3.49	3.89
Nb/Y	0.42	0.53	0.24	0.16	0.11	0.07	0.23	0.27	0.13
Nb/Ta	6.80	3.30	1.94	3.55	3.85	4.43	9.14	9.73	7.11
Ti/Sc	279.18	286.55	269.26	152.94	140.04	122.99	222.31	259.09	188.31
Zr/Sc	42.06	87.87	132.55	2.51	45.72	49.37	75.82	92.60	171.70

B	Borwar	Seliberi			Chitar			Chang
Field Code	19(d-)	20(c)	20(d)	20(e)	21(a)	21(b)	21(c)	22(a)
Processing Code	BO 4	SE 1	SE 2	SE 3	CHR 1	CHR 2	CHR 3	CHG 1
LOI	1.32	1.22	1.43	1.28	1.17	1.18	1.27	1.36
Th/U	6.94	9.59	9.15	13.05	8.09	12.38	10.38	11.16
Rb/Sr	1.82	5.75	6.19	5.30	0.80	1.08	0.90	11.44
Th/Sc	5.13	7.79	8.52	3.72	13.17	5.58	5.62	12.79
La/Sc	11.74	14.18	14.78	6.97	33.40	12.44	14.57	22.44
ΣREE	227.56	234.87	255.75	254.09	431.44	370.32	433.84	325.36
$(La/Yb)_N$	0.91	1.44	1.44	1.32	5.23	4.41	4.25	4.05
$(La/Sm)_N$	1.38	2.13	2.04	1.91	3.02	2.79	2.81	2.69
$(Gd/Yb)_N$	0.60	0.55	0.60	0.61	1.20	1.17	1.15	1.18
Eu/Eu*	0.45	0.36	0.33	0.32	0.34	0.41	0.38	0.21
Y/Nb	6.43	3.40	3.94	4.56	3.55	3.12	4.12	2.90
ASI	1.10	1.21	1.06	1.12	1.23	1.08	1.09	1.15
Ga/Al	3.68	3.74	3.67	3.56	3.27	3.69	3.56	3.56
Nb/Y	0.16	0.29	0.25	0.22	0.28	0.32	0.24	0.34
Nb/Ta	7.90	7.52	9.27	7.08	7.77	6.01	9.19	7.77
Ti/Sc	206.69	272.77	291.86	277.69	248.41	258.58	252.17	209.52
Zr/Sc	124.11	141.97	134.38	146.80	113.01	79.26	67.39	115.55

B	Chang			Balaram			Chiknawas		
Field Code	22(b)	22(c)	22(d)	23(a)	23(b)	23(c)	26(b)	26(c)	26(f)
Processing Code	CHG 2	CHG 3	CHG 4	BAL 1	BAL 2	BAL 3	CHW 1	CHW 2	CHW 3
LOI	1.21	1.27	1.25	1.19	1.34	1.45	1.30	1.39	1.13
Th/U	9.78	7.16	6.86	9.35	6.64	7.36	12.85	10.07	8.94
Rb/Sr	11.78	12.61	6.25	3.41	3.15	4.00	1.98	1.84	1.63
Th/Sc	11.93	19.53	7.88	4.92	5.44	3.94	8.17	41.90	9.17
La/Sc	23.53	28.05	15.44	11.86	10.59	10.70	16.65	23.34	22.54
ΣREE	370.85	305.87	444.18	362.03	234.18	328.94	296.46	347.25	166.08
$(La/Yb)_N$	4.00	2.59	3.56	9.91	8.33	8.33	11.09	10.22	12.99
$(La/Sm)_N$	3.12	2.80	2.92	3.66	3.32	3.34	4.21	2.49	5.26
$(Gd/Yb)_N$	0.96	0.73	0.94	1.79	1.66	1.65	1.75	2.48	1.55
Eu/Eu*	0.22	0.18	0.36	0.40	0.64	0.46	0.57	0.17	1.39
Y/Nb	4.18	4.31	4.34	2.86	2.92	3.19	3.72	4.16	3.45
ASI	1.06	1.06	1.00	0.96	0.97	0.88	1.08	1.19	1.10
Ga/Al	3.51	3.91	3.64	3.60	3.15	3.95	3.07	3.29	2.35
Nb/Y	0.24	0.23	0.23	0.35	0.34	0.31	0.27	0.24	0.29
Nb/Ta	7.39	9.30	5.28	9.70	6.65	9.24	6.75	4.92	3.50
Ti/Sc	241.38	329.93	262.32	467.22	424.29	324.02	661.62	448.07	386.22
Zr/Sc	141.51	179.23	95.83	100.25	99.96	119.53	132.44	89.38	112.46

C	Ranakpur	Borwar		Seliberi	Vagdadi			Chiknawas	
Field Code	16(b)	19(b)	19(e)	20(f)	25(a)	25(c)	25(e)	26(d)	26(e)
Processing Code	RAD 1	BOD 1	BOD 2	SED 1	VAD 1	VAD 2	VAD 3	CHWD 1	CHWD 2
LOI	1.46	1.25	1.18	1.25	1.32	1.11	1.35	1.26	1.28
Th/U	6.25	6.47	8.05	9.33	3.32	8.04	6.81	12.47	4.77
Rb/Sr	0.03	0.05	0.009	1.03	0.03	0.31	0.17	0.39	0.63
Th/Sc	1.00	0.15	0.96	1.09	0.06	0.26	0.28	0.37	0.18
La/Sc	3.34	0.26	6.36	2.50	0.64	1.06	1.29	1.73	0.89
ΣREE	221.64	140.41	368.98	181.42	76.31	203.35	202.40	300.08	186.50
$(La/Yb)_N$	13.33	0.90	29.32	7.59	8.17	6.30	6.04	7.76	4.81

(continued on next page)

Table 1B&C (*continued*)

C	Ranakpur	Borwar		Seliberi	Vagdadi			Chiknawas	
Field Code	16(b)	19(b)	19(e)	20(f)	25(a)	25(c)	25(e)	26(d)	26(e)
$(La/Sm)_N$	4.92	0.61	8.07	3.44	2.13	2.34	2.24	2.74	1.89
$(Gd/Yb)_N$	1.86	1.37	2.24	1.53	2.82	1.99	1.99	2.04	1.95
Eu/Eu*	0.65	0.75	0.67	0.61	1.18	0.79	0.82	0.80	0.85
Mg#	55.91	16.20	49.60	61.76	23.51	19.36	17.76	15.82	17.90

Table 2
Modal abundance (%) of Ambaji-Sendra Terrain granitoids.

	Tarpal			Ranakpur	Jaitpura		Borwar		
Field Code	15 (a)	15 (b)	15 (c)	16	18	18(b)	19(a)	19(c)	19(d)
Processing Code	TA 1	TA 2	TA 3	RA 1	JA 1	JA 2	BO 1	BO 2	BO 3
Quartz	34.2	38.4	35.1	22.5	35.5	37.1	42	36.2	40.3
Plagioclase	27.4	18.9	22.7	38.1	18.8	22.8	25.6	28.8	24.6
Orthoclase	12.1	4.3	16.4	6	8.9	6.3	5.8	6.5	9.3
Microcline	14	13.7	11.2	17.4	10.6	11.8	6.5	10.6	21.4
K- Feldspar	36.1	18.0	27.6	23.4	19.5	17.9	12.3	17.1	30.7
Biotite	2.2	22.2	14.3	0.0	24.6	18.3	10	9.4	0.0
Hornblende	8.3	0.0	0.0	14.6	0.0	0.0	8.7	6.3	0.0
Acc. Min.	1.8	2.5	0.3	1.4	1.6	2.7	1.4	2.2	4.4

	Borwar	Seliberi			Chitar			Chang
Field Code	19(d-)	20(c)	20(d)	20(e)	21(a)	21(b)	21(c)	22(a)
Processing Code	BO 4	SE 1	SE 2	SE 3	CHR 1	CHR 2	CHR 3	CHG 1
Quartz	35.5	38.3	35	33.6	42.2	37.7	39.1	38.2
Plagioclase	22.4	26.5	28.4	35.4	31.6	32.2	28.5	24.6
Orthoclase	8.8	11	10.9	6.2	11.5	4.8	7.6	9.5
Microcline	28.6	14.7	16.8	18.5	12.4	13.1	12.3	20.8
K- Feldspar	37.4	25.7	27.7	24.7	23.9	17.9	19.9	30.4
Biotite	0.0	6.4	4.5	3.8	0.0	9.5	10	4.2
Hornblende	0.0	0.0	0.0	0.0	0.0	0.0	0.0	0.0
Acc. Min.	4.7	3.1	4.4	2.5	2.3	2.7	2.5	2.7

	Chang			Balaram			Chiknawas		
Field Code	22(b)	22(c)	22(d)	23(a)	23(b)	23(c)	26(b)	26(c)	26(f)
Processing Code	CHG 2	CHG 3	CHG 4	BAL 1	BAL 2	BAL 3	CHW 1	CHW 2	CHW 3
Quartz	39.5	36.8	34.6	30	34.2	37.5	42.2	39.6	40.4
Plagioclase	41.2	32.5	25.8	37.5	29.8	32.4	36.5	33.8	37.6
Orthoclase	4.3	6.2	12.4	4.2	11.3	3.2	4.5	8.6	3.4
Microcline	10.8	18.4	22.2	22.4	21.9	24.6	12.8	15.2	18.2
K- Feldspar	15.1	24.6	34.6	26.6	35.2	27.8	17.3	23.8	21.6
Biotite	1.1	2.3	2.2	3.4	0.0	0.0	0.0	1.6	0.0
Hornblende	0.0	0.0	0.0	0.0	0.0	0.0	2.5	0.0	0.0
Acc. Min.	3.1	3.8	2.8	2.5	2.8	2.3	1.5	1.2	0.4

Chiknawas granites are magnesian to ferroan (0.78–0.90). Tarpal granites are Calcic and Alkali calcic (Na_2O + K_2O-CaO:3.83–8.25), Jaitpura granites are Calcic to Calc-alkalic (Na_2O + K_2O-CaO:5.79–7.11), Borwar, Seliberi, and Chang granites display Calc-alkalic (Na_2O + K_2O-CaO:5.83–7.88) nature, Chitar and Ranakpur granites are of Calcic character (Na_2O + K_2O-CaO:5.47–5.33), Balaram granites are Alkali calcic (Na_2O + K_2O-CaO:7.06–8.21) and Chiknawas granites posses Alkalic, Alkali calcic and Calcic varieties (Na_2O + K_2O-CaO: 5.77–10.94). According to alumina saturation index (A/CNK,) Jaitpura, Borwar, Seliberi, Chiknawas, Chitar granites are peraluminous (A/CNK:1.05–1.23), Tarpal and Chang granites are metaaluminous to peraluminous (A/CNK:0.55–1.26) and Balaram and Ranakpur granitoids are metaaluminous (A/CNK:0.88–0.95 Fig. 2, Table 1B).

In Ga/Al versus Zr and Nb diagrams (Whalen et al., 1987) majority of the samples of Ambaji – Sendra Terrain granites (ASTG) indicate their A-type nature (Fig. 3a,b). The (Zr + Nb + Ce + Y)–(Na_2O + K_2O)/CaO and (Zr + Nb + Ce + Y)-FeO^T/MgO diagrams also broadly confirm A-type nature of ASTG (Fig. 3c, d). The ASTG are classified as A2 based on their high concentrations of Y and Ce relative to Nb and high ratios of Ce/Nb and Y/Nb (>1.2) indicating presence of arc-like geochemical signatures (Eby, 1992). ASTG also have high Ta contents and thus low Yb/Ta ratio suggesting significant fluid interaction with the granitic melts (Table 1B).

Close scrutiny of elemental ratios particularly involving traces elements and REEs reveals that mineralogical division of ASTG into two groups is justified. ASTG1 (foliated granites, *syn*-orogenic), display least to moderately fractionated REE profiles (La/Yb_N:0.91–3.83) with moderate sink at Eu (Eu*: 0.24–0.51). ASGT2 (porphyritic granites, likely post −orogenic) possess significantly fractionated REE patterns (La/Yb_N:1.32–31.55) coupled with steep sink to positive kink at Eu (Eu*: 0.17–1.39) (Fig. 7). In synchronicity with their REE fractionation, ASTG1 possess lower values of Th/U, Rb/Sr, Th/Sc, La/Sc, ASI and Ga/Al ratios compared to ASGT2. However, Y/Nb ratio of the ASGT1 is higher than ASGT2 (Table 1B). Despite similar shapes of PM profiles of ASTG1 and ASTG2, differences in the abundance of various elements are clearly reflected in the magnitude of negative anomalies at Ba, Nb, Sr, P and, Ti and corresponding positive anomalies of preceding and succeeding elements. (Fig. 7). The mineralogical and geochemical grouping of ASTG is further confirmed by their trace element relationships. Selected TTE, LILE and HFSE show moderate to strong positive covariation with Zr in ASTG1 and crude positive variation in ASTG2.

Immobile trace element based Nb–Y diagram indicates that crustal fluids played role in modifying the composition of ATSG as significant number of samples (Ranakpur and Tarpal) plot in arc field (Fig. 4).

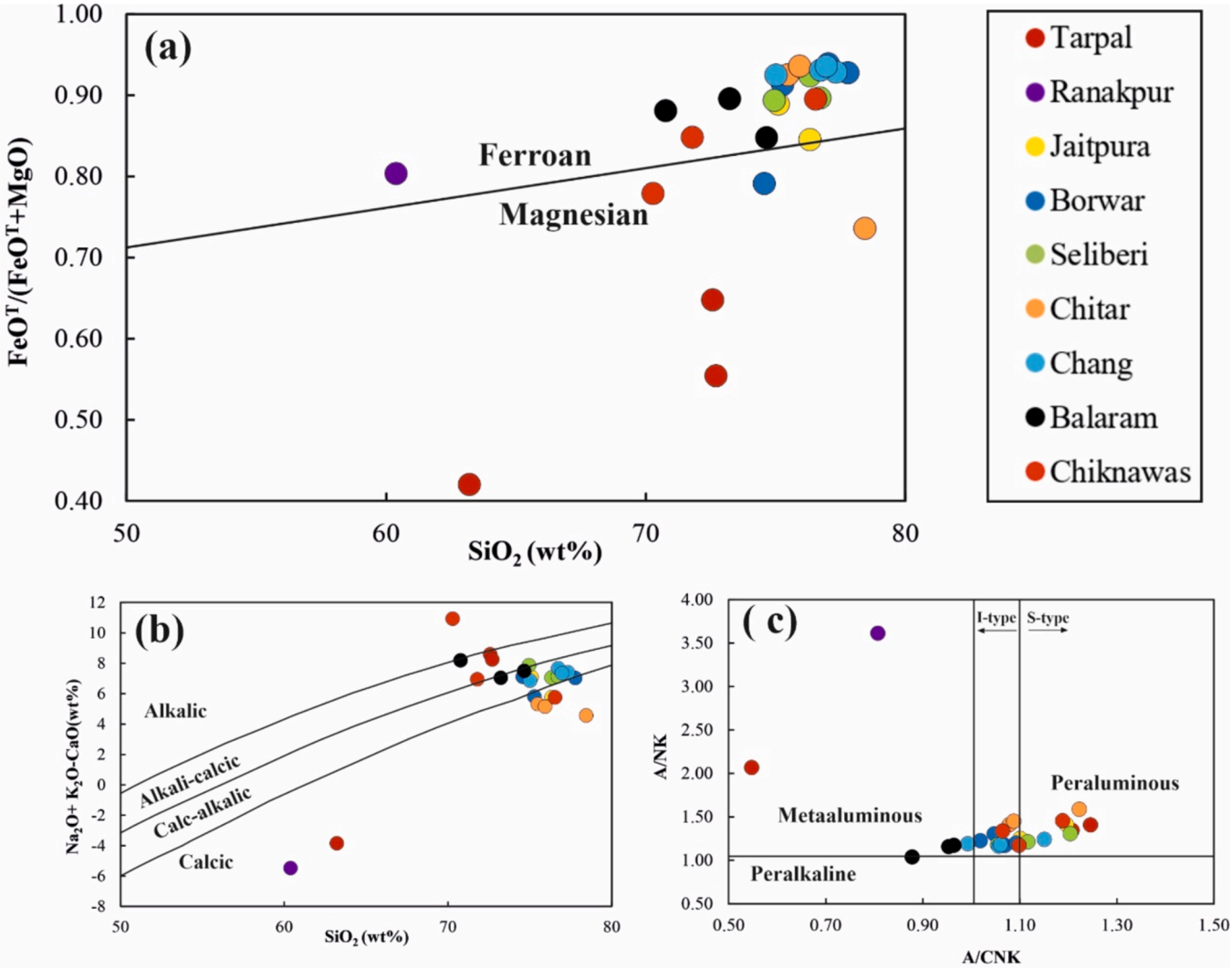

Fig. 2. (a)$FeO^T/(FeO^T + MgO)$ versus SiO_2 (b) Modified alkali-lime index: ($Na_2O + K_2O$-CaO) versus SiO_2 (Frost et al. 2001) indicating majority of AST granites are alkali-calcic to calc-alkalic. (c) Aluminium Saturation Index plot (after Maniar & Piccoli, 1989) classifying AST granites as largely peraluminous.

4.4. Petrogenesis of AST granitoids

A-type granites is a group of granitic rocks that is characterized by low water content and lack of orogenic or transitional tectonic fabric. They are classified in the S – I – A – M- or alphabetic system where 'A' stands for anorogenic or anhydrous. Compositionally A-type granites are highly ferroan and potassic and enriched in incompatible trace elements. They are also depleted in Sr and Eu, have high alkalies, high FeO/MgO and TiO_2/MgO ratios, and have high field strength elements (HFSE).

A-type granites are thought to be dominantly of non – crustal in origin. They are typically formed in stable intra-plate, back arc, or post collisional settings and be found in a variety of tectonic settings, including subduction zones, intracontinetal settings, and orogenic belts.

Nevertheless, the petrogenesis of A-type granites is still debated particularly for the nature of the potential source, e.g. granulitic sedimentary/igneous residue in the lower crust (Huang et al., 2011), underplated tholeiitic basalts and their derivatives (Wang et al., 2010) or a quartzo-feldspathic quartz–doritic–tonalitic– granodioritic source, as well as the role of the mantle (Wang et al., 2014).

Eby (1992) has shown that the Y/Nb ratio remains nearly constant during fractionation of A type magmas and thus serves as a key to identify the sources of magma. Granitic magmas with (Y/Nb < 1.2) are derived from the mantle source whereas higher ratios (Y/Nb > 1.2) imply solely crustal sources or mixed sources. Both groups of ATSG have Y/Nb > 1.2 suggesting their crustal origin. However, ASTG1 have very high Y/Nb ratios (2.27–14.4) compared to ASGT2 (1.88–4.56) advocating for their unequivocal crustal origin. This interpretation is well supported by various element ratios, A/CNK and trace element correlations with Zr in ASTG1 (Table 1B). Whereas, ASGT2 contain some mantle component as Zr does not vary positively with majority of elements except Sc advocating mafic mineral control over their composition.

It is thus interpreted on the basis of following points that metasomatized mantle-derived magmas also contributed in the generation of AST granites:

(1) Since Nb and Ta are less incompatible than Ce, Y and Yb during partial melting, melts generated in lower continental or upper continental crusts alone, should have higher Ce/Nb, Y/Nb and Yb/Ta ratios. ASTG1 and ASTG2 exhibit variably higher /lower or similar Ce/Nb, Y/Nb and Yb/Ta ratios compared to lower continental and upper continental crusts (Fig. 5c,d), preclude their derivation from a singular crustal source.
(2) REE contents in conjunction with trace element patterns differ in magnitude form continental crust. AST are enriched in HREEs, water soluble elements (i.e. Pb) and LILE which prescribe to them

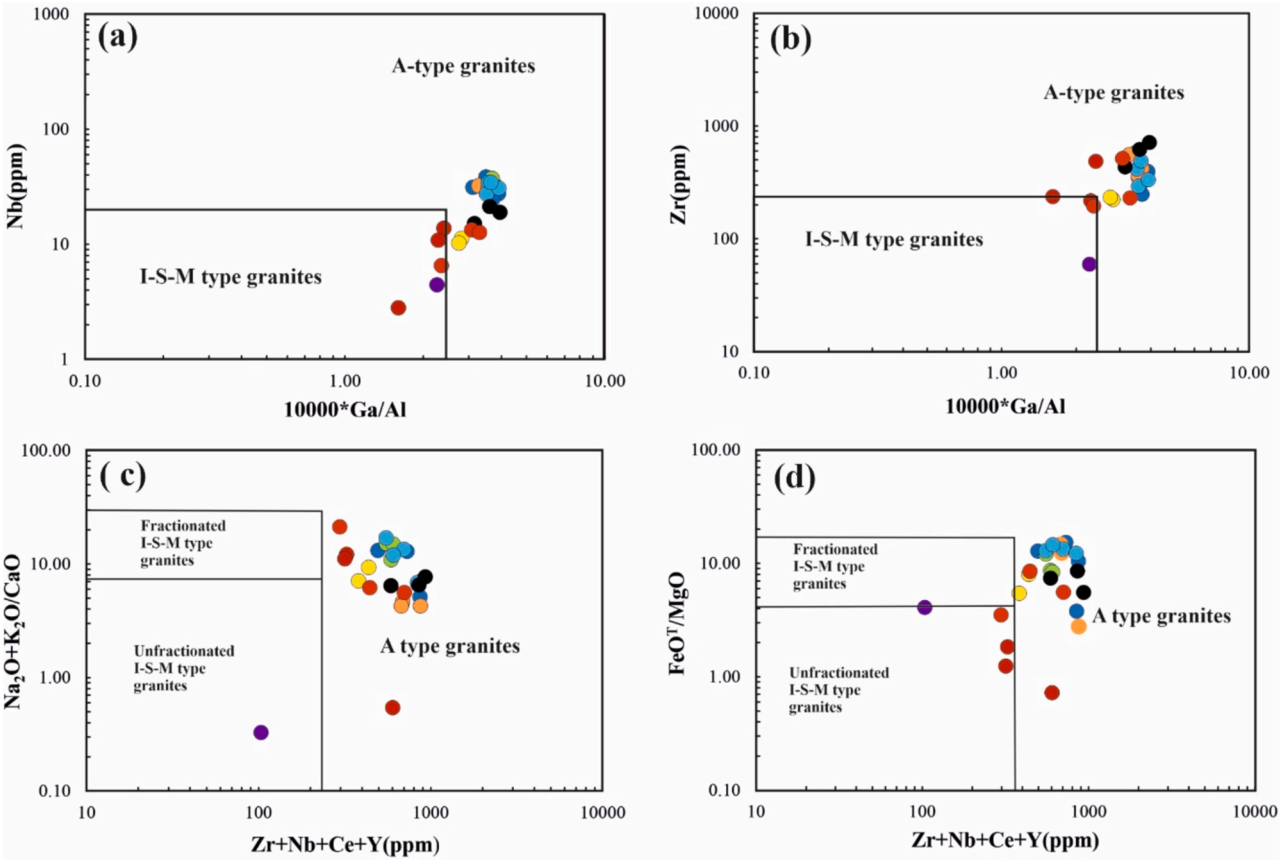

Fig. 3. Classification of AST Granites in (a) 10000*Ga/Al versus Nb (b) Zr, (c) (Zr + Nb + Ce + Y) versus ($K_2O + Na_2O$)/CaO and (d) (Zr + Nb + Ce + Y) versus FeO^T/MgO diagrams indicating their broadly unfractionated A – type nature (after Whalen et al., 1987). Legends as in Fig. 2.

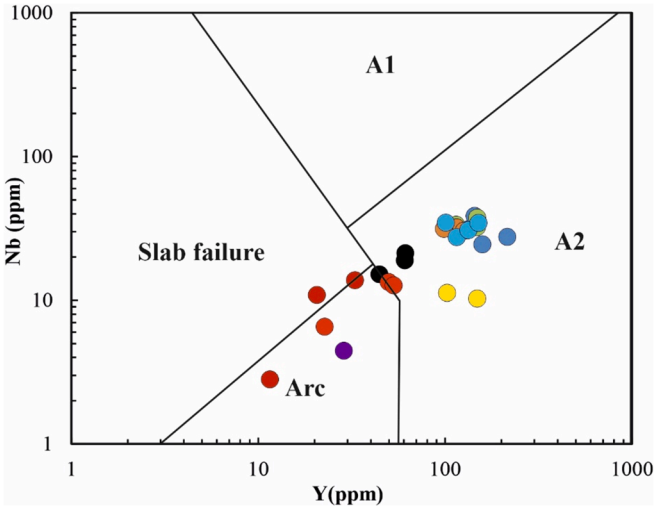

Fig. 4. Nb versus Y diagram suggesting arc to within plate setting to AST Granites (Whalen and Hildebrand, 2019). Legends as in Fig. 2.

a source metasomatized by the fluid originated from subducting slab.

(3) Nb/Ta ratio of ASTG is relatively low (ASTG1:2.5–9.26, ASTG2:1.94–9.7), compared to Cl-chondrite (17.57) (Sun and McDonough, 1989) and continental crust (Gao et al., 1998), indicating that low Nb/Ta ratio is their source characteristic. Such a source is expected to contain melt/fluid derived from the deep and high temperature subducted slab. It has been suggested that dehydration of hotter subducted slabs produce fluids which have subchondrite Nb/Ta ratios (Ding et al., 2009). The metasomatized mantle by low Nb/Ta bearing fluids, above the subducted slab, sustains its low Nb/Ta character. ATSG display Nb and Ti troughs in PM profiles (Fig. 7). Such Nb and Ti depletions, and other similar arc-type geochemical features in felsic rocks, have also been ascribed to anatexis of rocks derived through subduction processes.

Moreover, ratios like Ti/Sc, Nb/Ta etc of the ATSG show narrow variations, suggesting that the basement to the granites was largely monotonous or, alternatively, reflecting smaller amounts of crustal contamination implying intrusion through thin crust. The Nb/Ta and Ti/Sc ratios in ATSG are (1.94–9.3) and (133.6–644.5) respectively (Table 1B). As Sc is more compatible in the mantle than Ti, mantle sources typically produce higher Ti/Sc values than one would expect from a more felsic source. Furthermore, almost flat to slightly inclined HREE pattens of ASTGs in conjunction with high $(La/Yb)_{PM}$ and Zr/Y ratios and a pronounced negative Eu anomaly, preclude a garnet-rich, plagioclase-free residual phase (Zhang et al., 2023).

Log plots of Eu versus Ba and Sr for AST granites show gently inclined linear trends i.e. decrease in Ba and Sr contents with decreasing Eu concentration (Fig. 5e, f) which suggests constrained fractionation of feldspar in the evolution of these magmas wherein varying proportions of K-feldspar and plagioclase segregated through crystal fractionation processes. The evolution of A-type granites through feldspar fractionation is a global phenomenon because high temperature and in turn low viscosity promotes crystal fractionation in A-type magmas (Dall'Agnol et al., 2017).

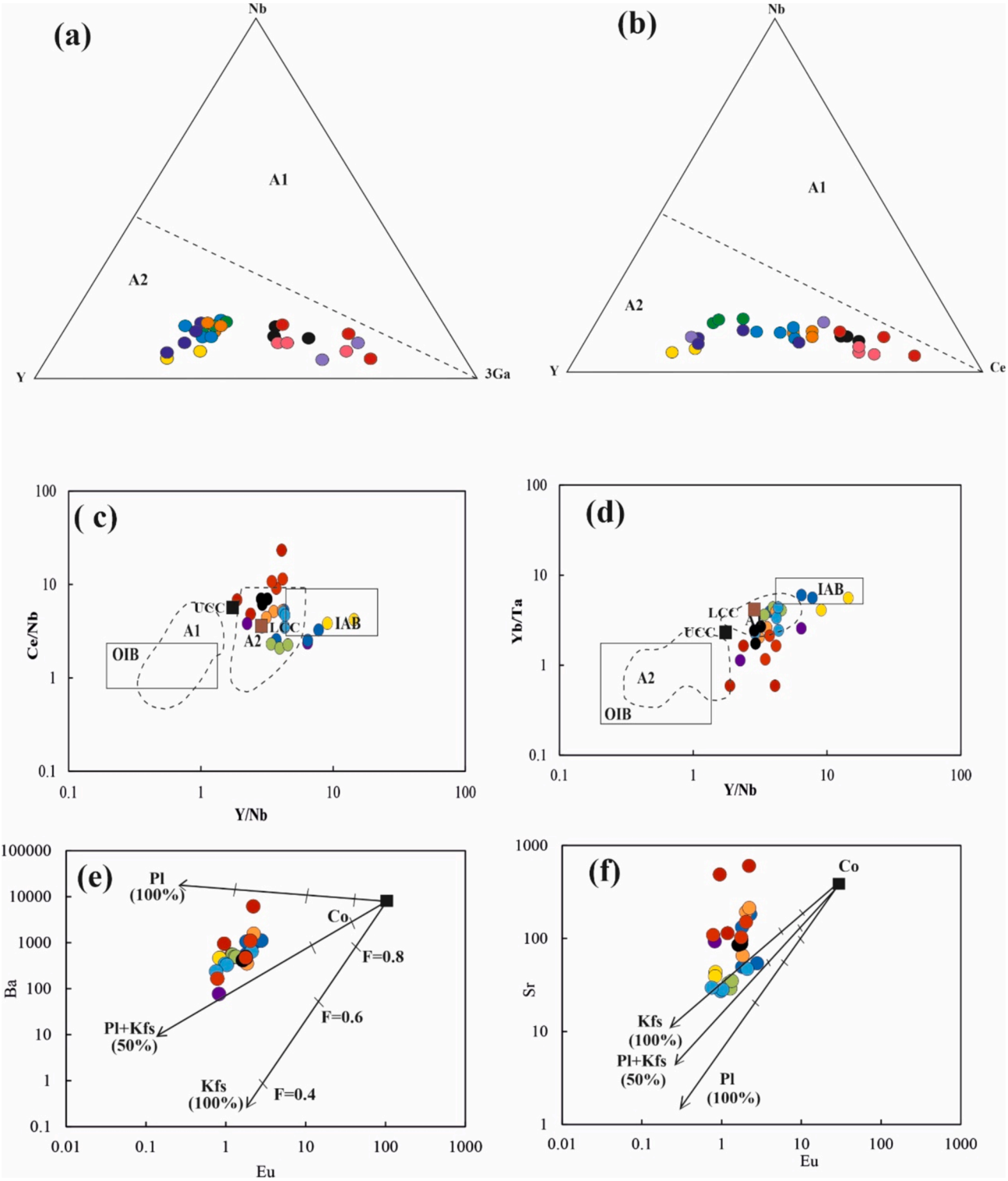

Fig. 5. Discrimination diagrams for A 1 and A 2-type granites (Eby, 1992). In (a) and (b) dashed line corresponds to Y/Nb ratio of 1.2. OIB –Oceanic island basalt, IAB – Island arc basalt. Log plots of Eu versus Ba (e) and Sr (f) for AST Granites indicating their generation by the fractionation of K – feldspar. Legends as in Fig. 2.

5. Ambaji-Sendra Terrain dykes

The magmatic rocks occurring as dykes in the granites of Ambaji – Sendra Terrain, herein referred to as Ambaji–Sendra Terrain Dykes (ASTD) are fine to coarse grained, largely holocrystalline, sub-ophitic/ophitic to occasionally porphyritic and composed of plagioclase, hornblende and iron minerals (magnetite/ilmenite). In volcanics groundmass is composed of slender tabular plagioclase, olivine, augite, amphibole, minor biotite. rutile and ± interstitial quartz. Plagioclase crystals occur as small subhedral to euhedral laths without any preferred orientation except in gabbros and dolerites.

ASTD appear to have suffered metamorphism upto the amphibolite facies grade. Their mineral assemblages containing combinations of hornblende, plagioclase, biotite and magnetite / ilmenite ± quartz are

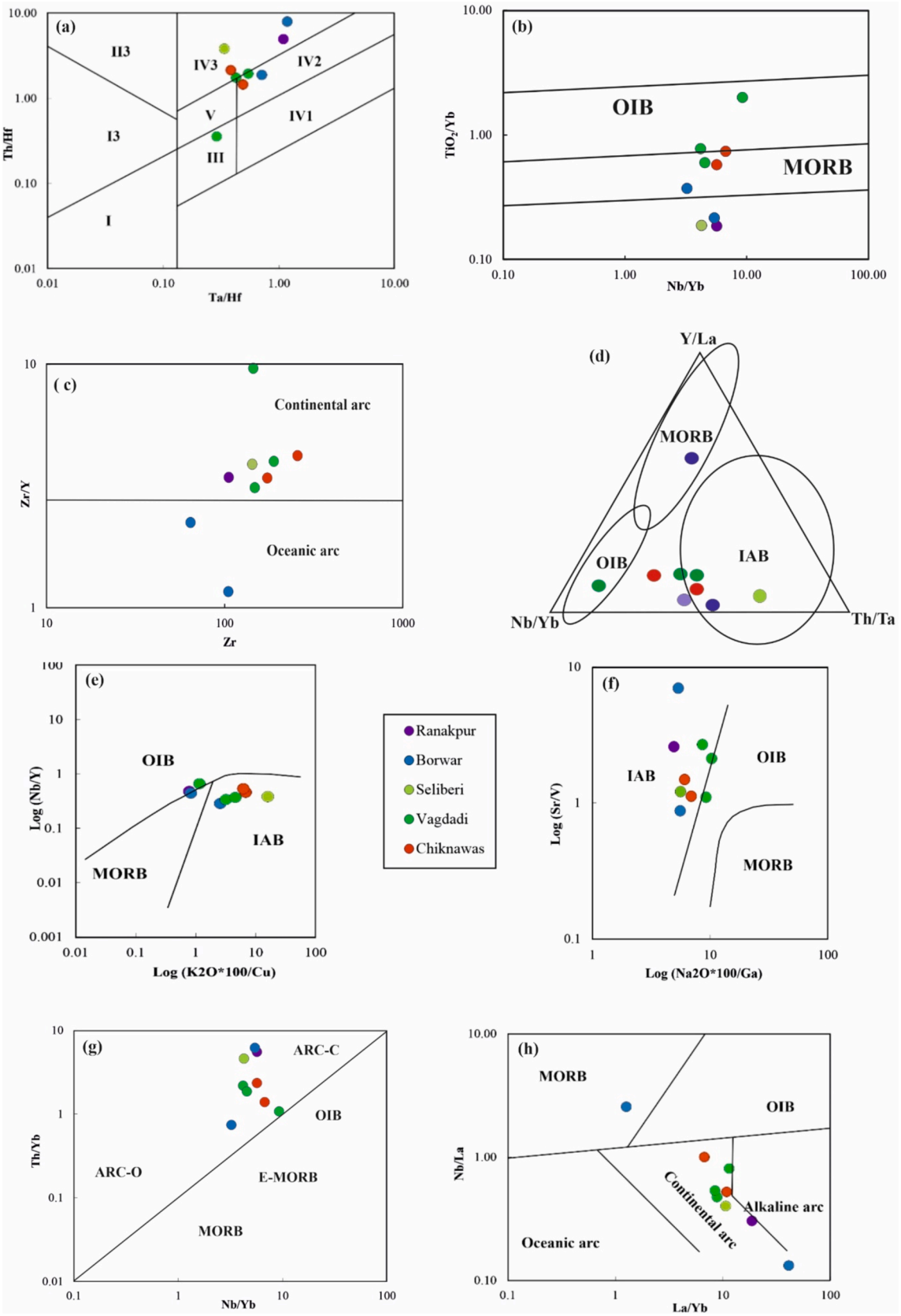

Fig. 6. Tectonic setting diagrams of AST Dykes. (a)Ta/Hf–Th/Hf (Wang et al. 2001): I. Divergent plate margin MORB; II. Convergent plate margin basalts; III. Oceanic within-plate basalts; IV. Continental within plate basalts; IV1: Intra continental rift + continental margin rift tholeiites; IV2: Intra continental rift alkali basalts; IV3: Continental extensional zone/initial rift basalts); V. Mantle plume basalts, (b) TiO_2/Yb (Pearce, 2008), (c) Zr − Zr/Y (Pearce, 1983), (d)Y/La-Nb/Yb-Th/Ta (e)Nb/Y vs $K_2O \times 100$/Cu, (f)Sr/V vs ($Na_2O \times 100$/Ga)(g) Nb/Yb − Th/Yb (Pearce, 2008) and(h) La/ Yb − Nb/La (Hollocher et al., 2012) showing within plate to arc character of AST Dykes.

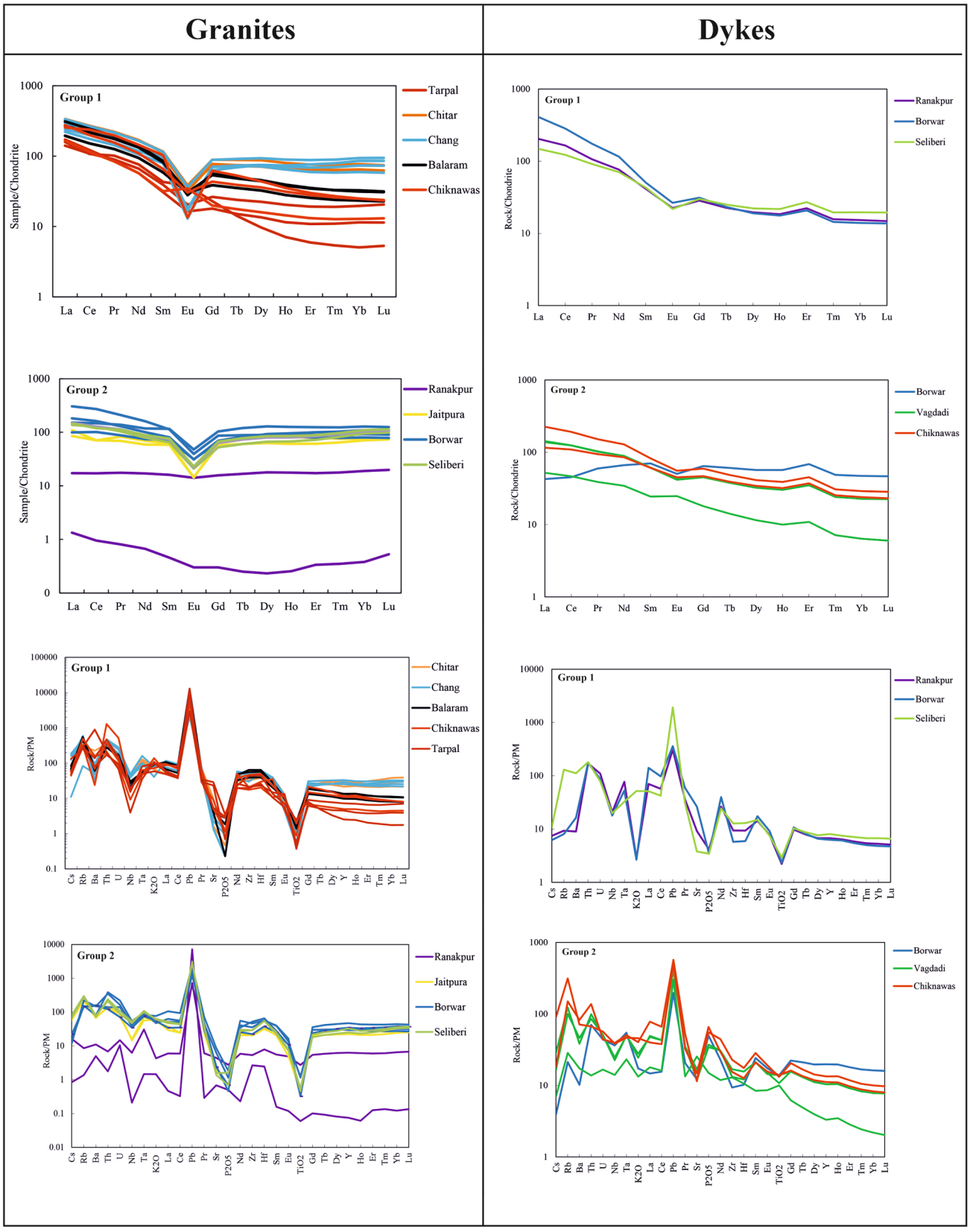

Fig. 7. Chondrite normalized REE diagrams and Primitive mantle (PM) normalized multielement diagrams for two groups of AST Granites and dykes. Normalizing values after McDonough and Sun (1989).

the testimony of this metamorphic grade. Relict primary minerals like olivine and augite are often seen in the thin sections.

5.1. Geochemistry of AST dykes

ASTD have very constrained values of loss on ignition (1.11–1.46 wt %). These values, in combination with field and petrographic observations, suggest that these rocks have not undergone any significant degree of alteration. The relationships between the resistant element Zr and LILE, TTE and HFSE are largely magmatic which further testifies that the chemistry of the dykes is almost undisturbed. Robust molecular ratio plots (figure not shown) devised to constrain elemental mobility of metavolcanics overwhelmingly indicate primary chemistry of ASTD even for alkalies.

SiO_2 values of ASTD, range from 49.81 to 53.94 wt% except Ranakpur and Seliberi dykes (56.86 wt% and 61.77 wt% respectively). Al_2O_3 generally varies from11.11 to 14.31 wt% except Seliberi (9.67 wt %) and a sample (VAD 3) from Vagdadi (16.35). Fe_2O_3 and MgO contents show inverse relationship in ASTD. Ranakpur, Seliberi and Borwar dykes are characterized by lower Fe_2O_3 (<7 wt%) coupled with higher MgO (>7 wt%) whereas in rest of the samples Fe_2O_3 is more (>13 wt%) and MgO is less (< 4 wt%). CaO content is significantly high in Ranakpur, Borwar and Seliberi dykes (11.04–18.68 wt%) compared to Vagdadi and Chiknawas dykes (6.13–7.26 wt%). Na_2O concentration is generally more than K_2O but is reverse in Seliberi and Chiknawas dykes. A significant feature of ASTD, particularly of Borwar, Vagdadi and Chiknawas dykes is their high TiO_2 and P_2O_5 contents which indicates presence of accessory minerals like ilmenite, rutile and apatite. This observation is duly endorsed by their petrography. The Mg# of ASDT (0.47–0.85) indicates their fractionated to evolved nature, corresponding to their transition from magnesian tholeiite (Mg# = ~80) to Fe-rich tholeiite (Mg# = ~50).

The relationships between immobile elements and Mg# and Zr suggest that ASDT are not primary melts and have experienced fractionation prior to emplacement in olivine + pyroxene + plagioclase sequence.

ASTD has variable but relatively high concentrations of TTE indicating control of mafic minerals such as pyroxenes. Sr and Ba contents are high and HFSEs are in moderate concentrations compatible with basalt chemistry. REE profiles of ASTD are nearly identical in shape with variable LREE enrichment (La/Yb_N:0.91–29.32). It is worth mentioning here that REE profile of two Borwar samples is like MORB (La/Yb_N:0.91) whereas its another sample is highly HREE fractionated (La/Yb_N:29.32). All ASTD samples show moderate to modest sink at Eu (Eu/Eu*:0.61–0.85) except VAD1 (Eu/Eu*:1.18) indicating variable plagioclase fractionation (Fig. 7).

PM normalized diagrams of ASTD show general enrichment of Rb, Th, Ta, Pb coupled with depletion in Ba, Nb, K and Ti of variable magnitude. Some samples of Ranakpur, Borwar and Seliberi dykes show significant depletion of P_2O_5 whereas all other samples are P_2O_5 enriched (Fig. 7).

5.2. Classification of AST dykes

Total Alkali-Silica, Zr/TiO_2-Nb/Y and YTC (Y:Y + Zr, T:TiO_2*100, C: Cr) diagrams classify ASTD as subalkaline rocks of basaltic to basaltic-andesite character with tholeiite to calcalkaline affinity indicating some role of subduction mechanism in their magma genesis.

Conventional discrimination diagrams give conflicting results about tectonic setting of ASTD varying from continental rift, oceanic basalt, continental arc to oceanic arc affinity (Fig. 6). Effectiveness of these discrimination diagrams have been questioned and debated by many researchers. Doucet et al. (2022), who observed that primary reason for such shortfalls stems from the fact that BABB, OFB, CFB and ARC-C environments exhibit mixed geochemical signatures due to localized factors, such as crustal and/or lithospheric contamination as well as their plate tectonic based origin i.e. arc settings. When ASTD data is plotted in more robust diagrams devised by Zhang et al. (2019), a broad IAB setting results for ASTD (Fig. 6e,f). Integration of the inferences adduced from Zhang's diagrams and conventional discrimination diagrams e.g. Nb/Yb − Th/Yb (Pearce, 2008) and La/ Yb-Nb/La (Hollocher et al., 2012) (Fig. 6g,h) a continental arc setting for ASTD appears to be most convincing interpretation. PM normalized REE profiles of ASTD is another testimony for their continental arc character (Fig. 7).

Verma (2009) has pointed out that the Nb value is critically influenced by the tectonic setting. $(Nb/Nb^*)_{PM}$ values, $[\{2\times(Nb_{sa})/Nb_{pm})/\{(Ba_{sa})/Ba_{pm})\} + \{(La_{sa})/(La_{pm})\}]$, where sa: concentration of element in sample, PM: concentration in the primitive mantle] in ASTD are 0.23–2.91. In intra-plate basalts this ratio is 0.25–0.70. Geochemical parameters, such as $TiO_2 \geq 2$ wt% and $P_2O_5 \geq 1$ wt% contents and $(Nb/Y)/(Zr/P_2O_5 \times 10000)$ ratio >1 indicate an intra-plate setting for ASTD (Winchester & Floyd, 1975). The within-plate affinity in conjunction with subduction signatures suggests that AST volcanism took place in a post-collisional continental geodynamic setting. Volcanism was probably driven by mantle convection processes which, in turn, might have been triggered by a late stage slab steepening or break-off beneath the Phulad ophiolite zone.

5.3. Petrogenesis of AST dykes

ASTD can also be divided into two groups. ASTD1 (Ranakpur, Seliberi and Borwar) are distinct from ASTD2 as displayed by their markedly lower concentrations of $Fe_2O_3^T$ (4.33–6.93 wt%), TiO_2 (0.48– 0.63 wt%) and P_2O_5 (0.15–0.18 wt%), higher MgO (6.97–8.11 wt%), CaO (11.04—18.68 wt%), and silica contents (52.34–61.77 wt%). ASTD1 is also depleted in TTE, LILE (except Th, U) and HFSE but contains higher concentrations of REEs. Whereas ASTD2 (Borwar – BOD1, Vagdadi and Chiknawas) are characterized by lower SiO_2 (49.81–53.94 wt%), MgO (2.97–6.1 wt%), CaO (6.13–11.57 wt%), and significantly higher $Fe_2O_3^T$ (13.17–16.8 wt%), TiO_2 (2.17–3.02 wt%), Al_2O_3 (11.11–16.35 wt%), Na_2O (1.35–2.3 wt%), K_2O (0.8–2.76 wt%) and P_2O_5 (0.65–2.86 wt%). Contrary to ASTD1, rocks of ASTD2 possess higher concentrations of TTE, LILE (i.e. Rb, Sr, Ba). These features of ASTD2 are similar to the Fe-Ti basalts which are characterized by iron- and titanium enrichment ($FeO^T > 12$ wt%, $TiO_2 > 2$ wt% and $FeO^T/MgO > 1.75$) coupled with silica depletion (Qian et al., 2006). The high Fe-Ti-P basaltic magma may be produced by several mechanism ranging from unmixing of magma, basaltic magma getting assimilated by Fe-Ti-P enriched rocks during its upward ascent, melting of pyroxenite mantle to produce Fe-Ti-rich primary magma which was later assimilated by P-rich rocks.

Since the ASTD do not have Fe-Ti oxides phenocrysts, the high concentrations of iron and titanium were not caused by the cumulus Fe-Ti oxides, and the Fe-Ti basalts may be interpreted to be products of moderate to high degree of Fenner trend differentiation of basaltic magma at low oxygen fugacity (Qian et al., 2006), to which a high P – rich rock or strange magmatic pulse enriched in P got assimilated. The cumulative product of this magmatic combination is the rocks ASTD2. However, ASTD1 possess unequivocal subduction signatures like negative Nb–Ta anomaly and enriched LILEs. When compared with primordial mantle, except Zr/Hf ratio, all other ratios of both groups are significantly higher or lower. Furthermore, despite possessing high MgO contents, ASTD1 are depleted in TTE but enriched in REEs compared with ASTD2 (Table 1C). These compositional differences between the two groups of ASTD refute their cogenetic origin either by fractional crystallization or crustal contamination of a common parental magma.

Sc is incompatible in olivine, plagioclase, and spinel, but is compatible in pyroxene, amphibole, and garnet. The presence of compatible minerals in the source would reduce Sc concentration in the magma. Niobium is a highly incompatible element in the mantle, but is highly compatible in rutile during plate subduction, which plausibly explains the typical Nb-Ta negative anomalies in IAB. Furthermore, IAB magmas are water rich which lowers the solidus line of plagioclase and

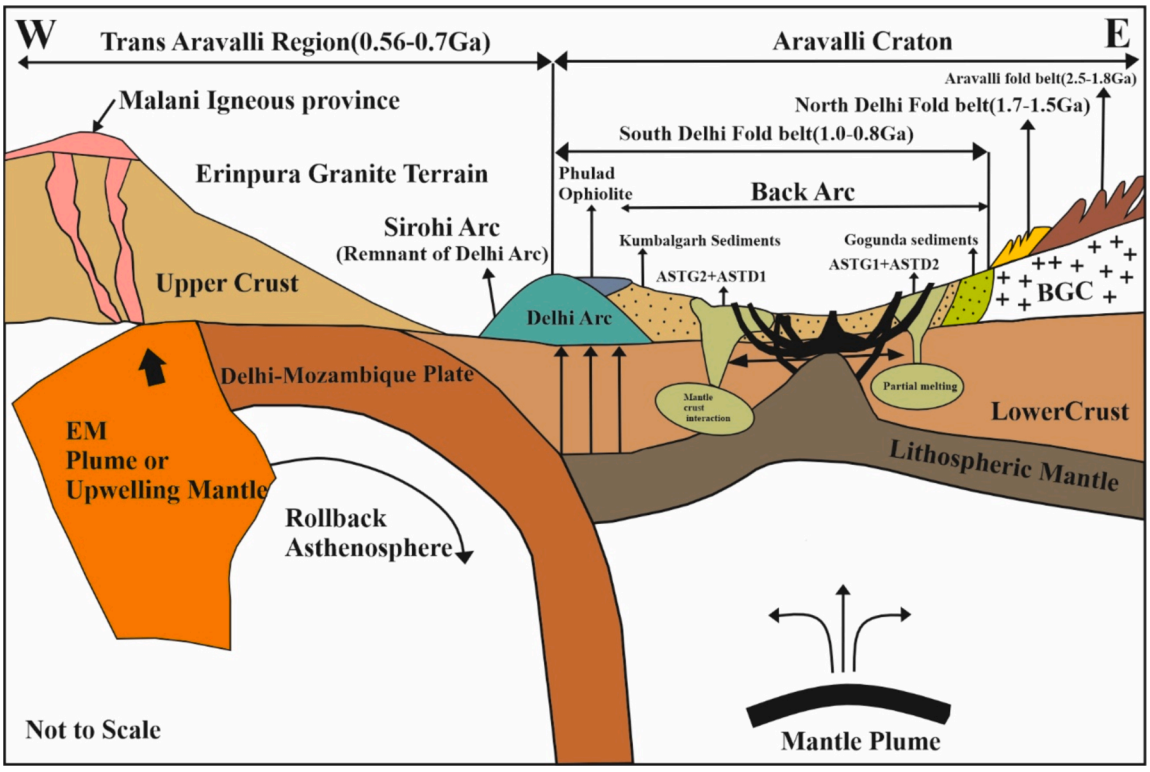

Fig. 8. Generalized sketch map illustrating the genesis of AST Granites and dykes and present-day distribution of various litho-components of Aravalli craton and Trans Aravalli Region (age brackets from multiple sources).

increases that of amphibole, so that amphibole crystalizes earlier than plagioclase (Alonso-Perez et al., 2009). All these signatures of IAB are nearly present in ASTD1. On the other hand ASTD2 possess some chemical features generally found in within-plate rocks.

Although it is difficult to define any chronological/stratigraphic hierarchy of the two groups of dykes, it appears convincing to believe that ASTD2 are relatively younger as they are disposed close to Kumbalgarh sediments (Delhi Supergroup) and associated with post orogenic porphyritic granites (ASTG2) whereas ASTD1 are in the vicinity of Phulad ophiolite in association with synorogenic foliated granite (ASGT1). Phulad ophiolite is considered to represent oceanic crust formed in island arc environment (Khan et al., 2019). It implies that ASTD1 and their host granites may be an extensional activity of oceanic closure. Alternatively, the continental arc, a possible tectonic setting adduced from the chemistry for ASTD, developed in the back arc setting. It seems reasonable to infer that ASTD1 was derived from magmas formed when the base of the previously metasomatized, volatile-mineral bearing subcontinental lithospheric mantle (Phulad mantle wedge) was heated by an upwelling mantle plume. ASTD2 were formed by partial melting of the rising plume head at a depth where garnet was stable, perhaps $>$ 80 km and got emplaced when back arc basin closed (i.e. a post collisional set up) as explained in Fig. 8.

6. Conclusion

ASTG originated from the magma generated at two different places in the lower crust both in consequence to the deep mantle upwelling. Magma for ASTG1 generated in the lower crust and passed through relative thick crust before intruding the Kumbalgarh sediments whereas ASTG2 magma generated at the lithospheric mantle – lower crust interface and passed through a thin crust. Further shallowing of lithospheric mantle during closure of Delhi ocean, generated mafic magma due to decompression melting which intruded ASTGs. Because of disposition of magma sources, dykes acquired within-plate (ASTD1) and arc characters (ASTD2). The process of emplacement of A-type (A2-subtype) AST granites and intrusion of mafic magma (ASTD) was initiated synchronously with Delhi ocean closure and culminated after the accretion of Delhi arc with North Delhi and Aravalli Fold belts as part of Rodinian assembly process. Identification of a remnant arc (Sirohi arc), in the Trans-Aravalli region is another testimony of this interpretation (Rao et al., 2013).

CRediT authorship contribution statement

Saima Rahman: Writing – original draft. **M. Shamim Khan:** Supervision. **Mohammed S. Fnais:** Writing – review & editing, Funding acquisition. **Tavheed Khan:** Formal analysis, Data curation.

Declaration of competing interest

The authors declare that they have no known competing financial interests or personal relationships that could have appeared to influence the work reported in this paper.

Acknowledgements

Authors thank Chairman, Department of Geology, AMU Aligarh, Director CSIR-NGRI, Hyderabad for providing necessary facilities. Authors express sincere thanks and gratitude to the Researchers Supporting Project Number (RSP2024R249), King Saud University, Riyadh, Saudi Arabia, for funding this research article. SR thanks CSIR, New Delhi for providing JRF & SRF [No. 09/112(0655)/2019-EMR-I] for carrying out this research. The authors sincerely acknowledge critical reviews by Prof. Z.S.A. Hamatteh and Prof. Gerald L. Chuwa which significantly improved quality and presentation of paper.

Appendix A. Supplementary material

Supplementary data to this article can be found online at https://doi.org/10.1016/j.jksus.2024.103524.

References

Alonso-Perez, R., Müntener, O., Ulmer, P., 2009. Igneous garnet and amphibole fractionation in the roots of island arcs: experimental constraints on andesitic liquids. Contrib. Miner. Petrol. 157 (4), 541–558.

Balaram, V., 2018. Recent advances and trends in Inductively Coupled Plasma - mass spectrometry and applications. Curr. Trends Mass Spect. 16 (2), 8–13.

Bhattacharjee, J., Golani, P.R., Reddy, A.R., 1988. Rift related bimodal volcanism and metallogeny in the Delhi Fold Belt, Rajasthan and Gujrat. India. J. Geol. 60, 191–199.

Dall'Agnol, R., da Cunha, I.R.V., Guimarães, F.V., de Oliveira, D.C., Teixeira, M.F.B., Feio, G.R.L., Lamarão, C.N., 2017. Mineralogy, geochemistry, and petrology of Neoarchean ferroan to magnesian granites of Carajás Province, Amazonian Craton: The origin of hydrated granites associated with charnockites. Lithos 277, 3–32.

Ding, X., Lundstrom, C., Huang, F., Li, J., Zhang, Z., Sun, X., Sun, W., 2009. Natural and experimental constraints on formation of the continental crust based on niobium–tantalum fractionation. Int. Geol. Rev. 51 (6), 473–501.

Doucet, L.S., Tetley, M.G., Li, Z.X., Liu, Y., Gamaleldien, H., 2022. Geochemical fingerprinting of continental and oceanic basalts: A machine learning approach. Earth Sci. Rev. 233, 104192.

Eby, G.N., 1992. Chemical subdivision of the A-type granitoids; petrogenetic and tectonic implications. Geology 20, 641–644.

Frost, B.R., Barnes, C.G., Collins, W.J., Arculus, R.J., Ellis, D.J., Frost, C.D., 2001. A geochemical classification for granitic rocks. J. Petrol. 42, 2033–2048.

Gao, S., Luo, T.C., Zhang, B.R., Zhang, H.F., Han, Y.W., Zhao, Z.D., Hu, Y.K., 1998. Chemical composition of the continental crust as revealed by studies in East China. Geochim. Cosmochim. Acta 62 (11), 1959–1975.

Gopalan, K., Macdougall, J.D., Roy, A.B., Murali, A.V., 1990. Sm-Nd evidence for 3.3 Ga old rocks in Rajasthan, northwestern India. Precambr. Res. 48, 287–297.

Gupta, S.N., Arora, Y.K., Mathur, R.K., Iqbaluddin, B.P., Sahai, T.N., Sharma, S.B., 1997. The Precambrian geology of the Aravalli region, southern Rajasthan and northeastern Gujarat. Memoirs Geological Survey of India 123, 262 p.

Hastie, A.R., Kerr, A.C., Pearce, J.A., Mitchell, S.F., 2007. Classification of altered volcanic island arc rocks using immobile trace elements: development of the Th - Co discrimination diagram. J. Petrol. 48, 2341–2357. https://doi.org/10.1093/petrology/egm062.

Heron, A. M., 1953. The geology of Central Rajputana. Memoirs of the Geological Survey of India (Vol. 79, p. 389). Delhi: The Manager of Publications.

Hollocher, K., Robinson, P., Walsh, E., Roberts, D., 2012. Geochemistry of amphibolite-facies volcanics and gabbros of the Støren Nappe in extensions west and southwest of Trondheim, Western Gneiss Region, Norway: a key to correlations and paleotectonic settings. Am. J. Sci. 312 (4), 357–416.

Huang, H.Q., Li, X.H., Li, W.X., Li, Z.X., 2011. Formation of high δ18O fayalite-bearing A-type granite by high-temperature melting of granulitic metasedimentary rocks, southern China. Geology 39 (10), 903–906.

Kemp, A.I.S., Hawkesworth, C.J., Foster, G.L., Paterson, B.A., Woodhead, J.D., Hergt, J. M., Gray, C.M., Whitehouse, M.J., 2007. Magmatic and crustal differentiation history of granitic rocks from Hf-O isotopes in zircon. Science 315, 980–983.

Khan, M.S., Smith, T.E., Raza, M., Huang, J., 2005. Geology, geochemistry and tectonic significance of mafic-ultramafic rocks of Mesoproterozoic Phulad Ophiolite Suite of South Delhi Fold Belt, NW Indian Shield. Gondw. Res. 8, 553–556.

Khan, M.S., Irshad, R., Khan, T., 2019. Geochemistry of Mafic-Felsic Rocks of Phulad ophiolite, in and around Pindwara-mount Abu region, South Delhi Fold Belt, NW Indian Shield: implications for its tectonic evolution. Geol. Evol. Precambrian Indian Shield 401–441.

Maniar, P.D., Piccoli, P.M., 1989. Tectonic discrimination of granitoids. Geol. Soc. Am. Bull. 101, 635–643.

Pandit, M.K., Carter, L.M., Ashwal, L.D., Tucker, R.D., Torsvik, T.H., Jamtveit, B., Bhushan, S.K., 2003. Age, petrogenesis and significance of 1 Ga granitoids and related rocks from the Sendra area, Aravalli craton, NW India. J. Asian Earth Sci. 22, 363–381.

Pearce, J.A., 1983. Role of subcontinental lithosphere in magma genesis at active continental margins. In: Hawkesworth, C.J., Norry, M.J. (Eds.), Continental Basalts and Mantle Xenoliths. Shiva Publication, Nantwich, pp. 230–249.

Pearce, J.A., 2008. Geochemical fingerprinting of oceanic basalts with applications to ophiolite classification and the search for Archean oceanic crust. Lithos 100 (1–4), 14–48.

Qian, Q., Gao, J., Xiong, X.M., Huang, D.Z., Long, L.L., 2006. Petrogenesis and tectonic settings of Carboniferous volcanic rocks from north Zhaosu, western Tianshan Mountains: constraints from petrology and geochemistry. Acta Petrol Sinica 22, 1307–1323 in Chinese with English abstract.

Radhakrishna, B.P., 1989. Suspect tectono-stratigraphic terrane elements in the Indian subcontinents. J. Geol. Soc. India v 34, 1–24.

Rao, C.D., Santosh, M., Kim, S.W., Li, S., 2013. Arc magmatism in the Delhi Fold Belt: SHRIMP U-Pb zircon ages of granitoids and implications for Neoproterozoic convergent margin tectonics in NW India. J. Asian Earth Sci. 78, 83–99.

Roy, A.B., Jakhar, S.R., 2002. Geology of Rajasthan (Northwest India) Precambrian to Recent. Scientific Publishers, Jodhpur, India, p. 421.

Sen, S., 1980. Precambrian stratigraphic sequence in a part of the Aravalli range, Rajasthan: A re-evaluation. Quart. J. Geol., Mining, Metall. Soc. India 52, 67–76.

Sinha-Roy, S., 1988. Proterozoic Wilson cycles in Rajasthan. Memoir Geological Society of India, 7: 95-108.

Sun, S.S., McDonough, W.F., 1989. Chemical and isotopic systematics of oceanic basalts: implications for mantle composition and processes. Geological Society, London, Special Publications 42 (1), 313–345.

Tiwana, J.K., Kaur, P., Chaudhri, N., 2022. Association of A-and I-type granitoids in the central Aravalli orogen, Rajasthan: Implications for the Neoproterozoic tectonic evolution of north-west India. Geol. J. 57 (8), 3267–3291.

Verma, P.S., 2009. Continental rift setting for the Central part of the Mexican volcanic belt: A statistical approach. – Open Geo. J. 3, 8–29.

Volpe, A.M., Macdougall, J.D., 1990. Geochemistry and isotopic characteristics of mafic (Phulad Ophiolite) and related rocks in the Delhi Supergroup, Rajasthan, India: Implications for rifting in the Proterozoic. Precambr. Res. 48, 167–191.

Wang, X.S., Hu, R.Z., Bi, X.W., Leng, C.B., Pan, L.C., Zhu, J.J., Chen, Y.W., 2014. Petrogenesis of Late Cretaceous I-type granites in the southern Yidun Terrane: New constraints on the Late Mesozoic tectonic evolution of the eastern Tibetan Plateau. Lithos 208, 202–219.

Wang, Q., Wyman, D.A., Li, Z.X., Bao, Z.W., Zhao, Z.H., Wang, Y.X., Chen, L.L., 2010. Petrology, geochronology and geochemistry of ca. 780 Ma A-type granites in South China: petrogenesis and implications for crustal growth during the breakup of the supercontinent Rodinia. Precambr. Res. 178 (1–4), 185–208.

Whalen, J.B., Currie, K.L., Chappell, B.W., 1987. A-type granites, geochemical characteristics, discrimination and petrogenesis. Contrib. Miner. Petrol. 95, 407–419.

Whalen, J.B., Hildebrand, R.S., 2019. Trace element discrimination of arc, slab failure, and A-type granitic rocks. Lithos 348–349, 105179.

Winchester, J.A., Floyd, P.A., 1975. Geochemical discrimination of different magma series and their differentiation products using immobile elements. Chem. Geo. 20, 325–343.

Zhang, B.C., Fan, J.J., Luo, A.B., 2023. Genetic pattern of the Albian volcanic rocks in the Ziruco area. Northern Tibet: Implications for A-Type Granites: Lithos 436–437. https://doi.org/10.1016/j.lithos.2022.106970.

Zhang, Q., Sun, W., Zhao, Y., Yuan, F., Jiao, S., Chen, W., 2019. New discrimination diagrams for basalts based on big data research. Big Earth Data 3 (1), 45–55.